Structural stability of naphthyl end-capped oligothiophenes in organic field-effect transistors measured by grazing-incidence X-ray diffraction in operando

Huss-Hansen, Mathias K.; Lauritzen, Andreas E.; Bikondoa, Oier; Torkkeli, Mika; Tavares, Luciana; Knaapila, Matti; Kjelstrup-Hansen, Jakob

Published in:
Organic Electronics

Link to article, DOI:
10.1016/j.orgel.2017.07.012

Publication date:
2017

Document Version
Early version, also known as pre-print

Structural stability of naphthyl end-capped oligothiophenes in organic field-effect transistors measured by grazing-incidence X-ray diffraction *in operando*

Mathias K. Huss-Hansen[a], Andreas E. Lauritzen[a], Oier Bikondoa[b,c], Mika Torkkeli[a], Luciana Tavares[d], Matti Knaapila[a,*], Jakob Kjelstrup-Hansen[d,*]

[a] *Department of Physics, Technical University of Denmark, 2800 Kgs. Lyngby, Denmark*
[b] *XMaS, The UK-CRG Beamline, European Synchrotron Radiation Facility, 38043 Grenoble Cedex 09, France*
[c] *Department of Physics, University of Warwick, Gibbet Hill Road, CV4 7AL, Coventry, UK*
[d] *NanoSYD, Mads Clausen Institute, University of Southern Denmark, 6400 Sønderborg, Denmark*

Abstract

We report on microstructural durability of 5,5'-bis(naphth-2-yl)-2,2'-bithiophene (NaT2) in organic field effect transistors (OFETs) *in operando* monitored by grazing-incidence X-ray diffraction (GIXRD). NaT2 maintains its monoclinic bulk motif in operating OFETs with $a = 20.31 \pm 0.06$ Å, $b = 6.00 \pm 0.01$ Å, $c = 8.17 \pm 0.04$ Å and $\beta = (96.64 \pm 0.74)^\circ$. Crystallites appear as a mosaic of single crystals reaching through the whole 50 nm thick active layer. The lattice parameters variation (<1%) falls within the statistical error of structure refinement when the OFET gate voltage is varied from 0 V to -40 V; or when the OFET is continuously cycled within this voltage interval over more than 10 h period. Within the first few cycles, both the hole mobility and threshold voltage are changing but then reach stable levels with an average mobility of $(3.25 \pm 0.04) \times 10^{-4}$ cm^2/Vs and an average threshold voltage of -13.6 ± 0.2 V, both varying less than 4% for the remainder of the 10 h period. This demonstrates crystalline stability of NaT2 in operating OFETs.

*Corresponding authors
Email addresses: matti.knaapila@fysik.dtu.dk (Matti Knaapila), jkh@mci.sdu.dk (Jakob Kjelstrup-Hansen)

Keywords: *in operando*, grazing-incidence X-ray diffraction, oligothiophene, organic TFT

---

1. Introduction

Organic field effect transistors (OFETs) constitute a key component in organic electronics [1, 2, 3]. Their advantages include large-area and inexpensive processing on a variety of substrates, low material consumption and flexibility. The OFET performance depends on the long range morphology and short range molecular packing as well as on macroscopic and microscopic defects, and materials with high degree of order are generally desirable [1, 2, 3, 4, 5]. Also extrinsic factors such as ambient humidity affects device performance [6]. A remaining challenge relates to the electrical stability or so-called bias-stress stability [7]. When OFETs operate under prolonged electrical bias, a continuous shift of the threshold voltage and therefore a change of the on-current is often observed. This is connected to the migration and trapping of charged species under the influence of the applied electric field, but the exact mechanism remains to be fully understood. The location of the traps has for example been suggested to be at grain boundaries of the organic layer [8, 9] or at the dielectric/semiconductor interface [10], and it has been determined that water plays a role [11, 12], even though the bias-stress also occurs under vacuum conditions. Recently Liscio and co-workers [13] employed grazing-incidence X-ray diffraction (GIXRD) to study pentacene OFETs *in operando*, and proposed that an applied electric field could reorient a fraction of the pentacene molecules located at or near grain boundaries leading to energy lowering and the formation of a shallow trap for charge carriers that would influence bias-stress stability.

Oligothiophenes used in OFETs show a rich variety of structural phenomena determining the OFET performance [14]. Typical oligothiophenes are either fused systems [15] or end-capped by alkyl [16] or aromatic or polyaromatic groups in a symmetric [17] or asymmetric manner [18] manifesting vertically aligned face-to-face structure on the OFET surface. This structure is further modified by an additional molecular layer between electrodes and thiophene layer [19] or altered by external parameters such as externally induced uniaxial strain [20]. The structure of various oligothiophenes in OFETs has been resolved *ex situ* even in the monolayer level [16] but the effect of electric field in running OFETs, corresponding those observed for pentance [13], are not well reported.

Geng and co-workers introduced naphthyl end-capped oligothiophenes with good stability and crystallinity as well as relatively high mobilities [21]. The end-capping helped to prevent side reaction, which hinders polymerization and oxidation and the high polarizability, amongst other beneficial properties for OFETs. The authors found that these materials are particularly stable and lose less than 1% of their weight when heated up to 325 °C or more. Among these materials, the crystal growth of 5,5'-bis(naphth-2-yl)-2,2'-bithiophene (NaT2) shows also a peculiar property as the molecules may form extremely high aspect ratio fibers, 20 nm thick and several micrometers long, when grown on muscovite mica, with potential in phototransistors [22] and waveguides[23]. Structures of these materials were characterized in the single crystal bulk but not in OFETs [21].

As the performance of OFETs depends on the thin-film structures, various aspects and processing steps of conjugated oligomers and polymers have been studied by GIXRD including alignment [24], phase behavior [25, 26], solution shearing [27], solvent vapour annealing [28], roll-to-roll processing [29], doctor-blading [30] and spray-processing in real time [31]. However, apart from the GIXRD studies of Liscio and co-workers [13] the GIXRD literature of OFETs *in operando* is less comprehensive.

In this paper we report on the structure and structural stability of NaT2 in operating OFETs. Our objectives are to study Na2T in the OFET environment; demonstrate the versatility of GIXRD when probing OFETs *in operando*; and seek for electric field induced effects like those reported by Liscio et al. [13]. We find NaT2 forming a mosaic of essentially monoclinic single crystals through the whole active layer. This structure remains stable with the lattice parameters varying less than 1% when running OFET 10 hours, thus confirming the stability assumption of Geng and co-workers.

2. Experimental

Fig. 1 shows the chemical structure of NaT2. The synthesis of NaT2 followed a Stille cross-coupling approach as described in Ref.[32].

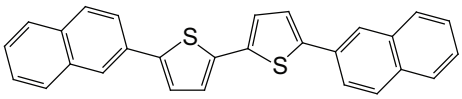

Figure 1: Chemical structure of NaT2

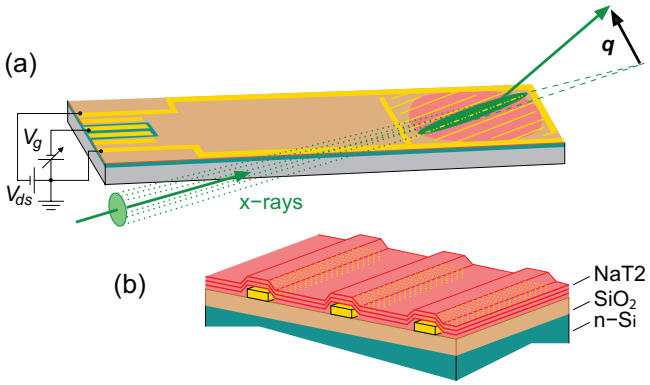

Figure 2: (a) Schematics of experimental settings and a bottom contact OFET electrode layout during GIXRD experiments and (b) the layered film profile above and between the source-drain electrodes. Not drawn to scale. The electrode width is exaggerated and the number of molecule layers is about 25.

Fig. 2 illustrates the experimental settings. The OFET layout consisted of a highly n-doped Si carrier substrate as a back gate electrode with a 200 nm thick thermally grown SiO_2 layer as the gate dielectric. On top, interdigitated source and drain electrodes were fabricated by E-beam evaporation of Ti/Au (3 nm/30 nm), structured by photolithography and lift-off processes. The gap between the source and drain electrodes (the transistor channel length) was 500 μm, while the width of each interdigitated finger of the source and drain electrodes was 20 μm. The transistor channel width-to-length ratio was 268.78 and the area covered by the interdigitated electrode pattern 10 mm $\times$ 10 mm. Finally, a 50 nm thick NaT2 layer was deposited by vacuum sublimation (deposition pressure 10^{-8} mbar, deposition rate 0.2

nm/s) on top of the transistor substrates. In this configuration, the gold electrodes occupied only a minor part of the transistor area (4%) and most of the active film was therefore deposited on the SiO_2 surface. The sample was designed to fit into a ZIF (zero insertion force) socket for electrical connections to allow for easy sample exchange in GIXRD experiments.

GIXRD measurements were carried out at XMaS (BM28), the UK CRG beamline at the European Synchrotron Radiation Facility (ESRF) in France. A nylon/metal-printed sample chamber filled with Helium was used to reduce background due to air scattering [33]. The X-ray energy was 10 keV and the beam size 100 μm $\times$ 260 μm (vert. $\times$ hor.). Depending on the given measurement, the incidence angle varied nominally from 0.20° to 0.50°. The sample-to-detector distance was determined by a silver behenate calibration sample as well as by monitoring the position of the direct X-ray beam on the detector as a function of detector angle relative to the incident beam. A partially transparent beamstop allowed trace the attenuated direct beam on the detector. The electrode length was about 14 mm at the X-ray beam position and the X-ray footprint 11.5 mm for an incidence angle of 0.5°. X-ray images were collected with an MAR 165 charge-coupled device (CCD) detector. Samples were mounted onto a PCB slot to allow electrical connections. *In operando* electrical measurements were carried out by biasing the transistor with programmable voltage supplies (Kepco and HP) and recording the resulting current with a Keithley picoammeter.

Two types of *in operando* measurements were performed. In the first type, a fixed V_{ds} (e.g -20 V) was applied to the sample while the gate electrode was grounded (i.e. the transistor was off) followed by an instantaneous GIXRD measurement. Next, a gate voltage of the same value as V_{ds} was applied and after a period of time of 120 s a new GIXRD measurement was made. After this, all bias voltages were set to zero. This measurement protocol was then repeated – next time applying a V_{ds} of -30 V, and in the last step of -40 V. This protocol was used to show whether the gate voltage had significant effect on the lattice parameters.

The second type of electrical measurement was an ageing test in which the transistor was cycled between off and on states over approximately ten hours. In this measurement, a fixed V_{ds} was applied throughout the measurement sequence while the gate voltage was varied to cycle between the off and

on states. Initially, a gate voltage of 0 V is applied (transistor off), and a GIXRD image was taken. The gate voltage was swept from 0 V to -40 V (while recording the current in order to be able to extract electrical transistor parameters), and a subsequent GIXRD measurement was again made after a stabilization period of 120 s while the transistor was on. Next, the gate voltage was scanned back to 0 V and the protocol immediately repeated and this continued for 10 hours. This protocol was to study the materials durability in operating OFETs.

The raw images were converted from the pixel space into the $\mathbf{q}$ space as described in Ref. [34]. This procedure determines the effective detector angles for each detector pixel. These effective detector angles for each pixel are related to the vectors in the reciprocal space in the horizontal geometry as

$$\mathbf{H}_{\varphi} = \begin{bmatrix} X \\ \cos\omega_h Y + \sin\omega_h Z \\ \cos\omega_h Z - \sin\omega_h Y \end{bmatrix}, \quad (1)$$

where (X, Y, Z) is the momentum transfer in the laboratory frame and ω_h the sample tilt as shown in Fig. 1 in Ref. [34]. In our experiment the sample rotation $\varphi = 0$. This procedure accounts the tilted detector angles and the curvature of the Ewald sphere. The peak positions on the converted images were found by fitting cuts along $\mathbf{q_z}$ and $\mathbf{q_{xy}}(= \sqrt{X^2 + Y^2})$.

The conversion of q-values to the exact thin film lattice parameters in a textured sample requires acquiring pole figures as discussed in Ref.[35]. Obtaining full pole figures is impractical for our *in operando* measurements with fixed electrical connections (Fig. 2). In order to detect possible texture in-plane, the samples were rotated 90° about the sample surface normal. The resulting GIXRD images were identical for both directions and the diffraction peaks and the lattice parameters matched very well to those calculated from single crystals (*vide infra*). Thus the texture correction was deemed not necessary and the procedure allowed us to detect relative changes in lattice parameters as a function of time, voltage or incident angle.

The lattice parameters a, b, c and β of NaT2 were refined using weighted nonlinear regression from 6 of the 25 resolved peak positions, corresponding to Miller indices (200), (300), (011), (111), (102) and (202). Previously reported lattice parameters for single crystal NaT2 were used as an starting

point for this procedure [21]. The fitting error is calculated from the diagonal of the estimated variance-covariance matrix and given as $\pm$ 1 standard deviation. The crystallite size along **z** direction was estimated from the width of (100) arc.

The saturation hole mobilities and threshold voltages were obtained by fitting to the measured electrical transfer characteristics.

3. Results and discussion

3.1. NaT2 structure in OFETs.

Fig. 3 shows a typical 2D GIXRD pattern and the proposed indexation of NaT2 in an operating OFET. Fig. 4 shows selected layer intensity profiles deduced from the 2D GIXRD patterns. Also shown are the calculated peak positions and scattering intensities (vertical bars) for various Miller $hk\ell$ indices using the single crystal NaT2 structure reported in the CSD database (644331.cif from Ref [21]). In the grazing incidence geometry the detector does not observe the central region of the $h00$ reflections and so only the calculated intensities are shown. The three observed layer lines, ($h10$) ($h11$) and ($h02$), have been shifted vertically for clarity. Figure 4 illustrates the NaT2 unit cell and the proposed unit cell packing in the OFET geometry as well as the relation between direct and reciprocal space.

The GIXRD pattern shows an array of sharp peaks and the pattern is identical if the sample was rotated 90° about **z** axis, *i.e.*, the incident beam transversed perpendicular to the electrodes. Our refinement provides the lattice parameters $a = 20.31 \pm 0.06$ Å, $b = 6.00 \pm 0.01$ Å, $c = 8.17 \pm 0.04$ Å and $\beta = (96.64 \pm 0.74)°$. The refined parameters are close to those reported to the single crystal and the similarity between the unit cells in bulk and in OFET is supported further by similar peak intensities (Fig. 4). These observations together with the fact that the approximated crystallite size along **z** direction (∼40 nm) corresponds to the 50 nm film thickness indicate that NaT2 appears essentially as a mosaic of single crystals reaching through the whole active layer. This means that the **a** axis nearly follows the **z** axis whereas the *bc*-plane of adjacent crystallites has no correlation along the surface normal. In order to detect possible crystallite orientation in-plane, the samples were rotated 90° about the sample surface normal. The GIXRD images were identical for both directions.

This structure should be compared to the thin film structure of asymmetrically substituted 5-(4-decylphenyl)-5'-(naphthalen-2yl)-2,2'-bithiophene (DP2TN) which contains two thiophene rings end capped by a naphtyl group in one end and by a decylphenyl group in another end [18]. Both molecules are seemingly rigid rods and vertically packed but the packing on surfaces is significantly different. The flexible alkyl chains of DP2TN seem to lower the degree of order in plane and this is manifested in the GIXRD data by verti-

cal streaks (Bragg rods) characteristic for a liquid crystalline like order. The Bragg rods are also observed in pentacene films [13]. Similar streaks are not observed for NaT2 but the peaks are equally resolved for all three directions. Thin film structure of fluorene-bithiophene-fluorene (FTTF) is another relevant analogue where naphtyl end groups of NaT2 are replaced by fluorene groups [17]. FTTF forms rectangular unit cells but crystallites are initially not well oriented on the surface as indicated by the diffraction rings rather than peaks. The orientation is significantly improved and sharp peaks are resolved by increasing the deposition temperature from room temperature to 90 C°. This illustrates a delicacy in the crystal growth of bithiophenes.

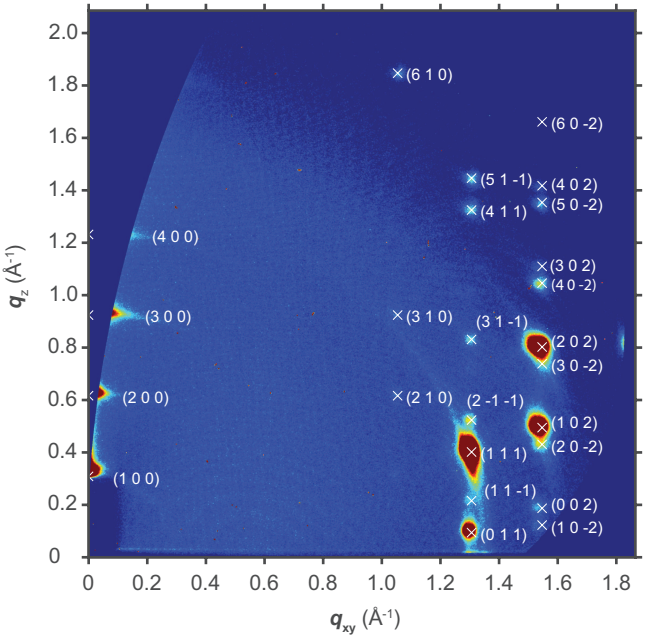

Figure 3: 2D GIRXD pattern of NaT2 on a running OFET. The $\boldsymbol{q}$ vectors correspond to the setting shown in Fig. 4 (*vide infra*).

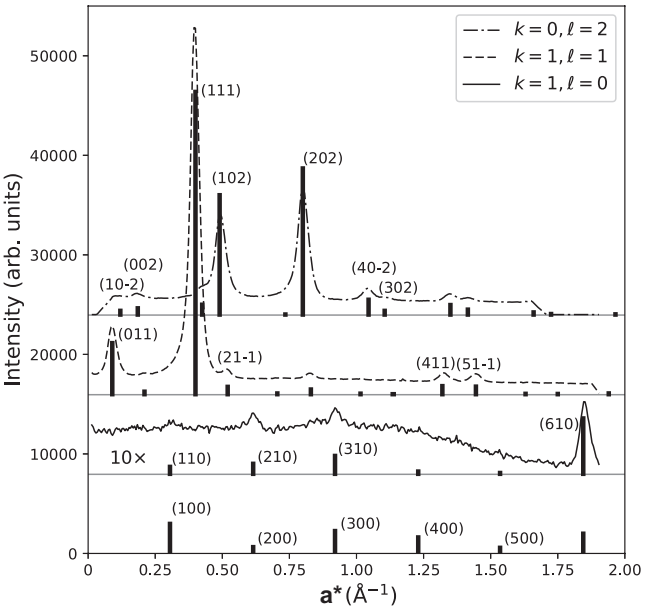

Figure 4: Selected $kl0$ lines of NaT2 GIXRD data (dotted and dashed, dashed and solid lines) and the peak positions and scattering intensities calculated from the single crystal data of Ref. [21] (histograms).

Fig. 6 shows the lattice parameters as a function of V_g at the 0.25° incidence angle when V_{ds} is kept equal to V_g (and when 4% of the measured film is actually on top of the electrodes). The refined monoclinic angle varies less than 8 mrad when the field is turned on. However, the statistical accuracy of refinement is actually larger, 17 mrad. Thus, the molecular structure remains essentially stable within the 2% limits. This implies that an electric field of around 10^8 V/m does not influence NaT2 or the effect is not measurable by our instrumentation.

This result should be compared to the pentacene structure [36, 37] and to the work of Liscio et al. [13] who reported a molecular tilt toward the direction of the applied field. The reason for this may be attributed to differences in the order. The difference of their structure is manifest as the absence of maxima along the Bragg rods. While pentacene shows good 2D order within the layers, the layer-to-layer structure is weaker. This simple difference may account to the molecules being easier to align due to the bias stress. This is also in line with the observation that Liscio and co-workers did not ob-

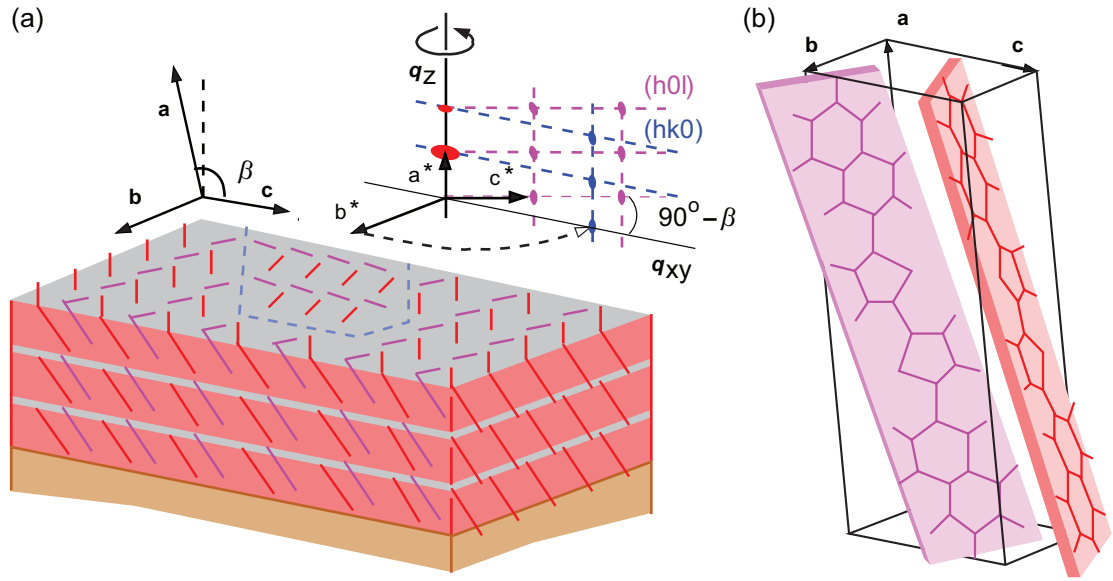

Figure 5: Illustrations for (a) NaT2 film and (b) NaT2 unit cell on OFETs. Vectors $\mathbf{q_z}$ and $\mathbf{q_{xy}}$ follow the experimental geometry while **a**, **b**, and **c** and **a***, **b*** and **c*** represent the basic vectors of the direct and reciprocal lattices, respectively.

serve similar change in the crystal structure for thicker films (50 monolayers) which is more comparative to our case. The NaT2 films on the other hand are well ordered crystallites that show no indication of surface effects to the structure. Thus we may conclude that bias-stress plays no significant effect on NaT2 where the crystalline order is good in all three directions.

Fig. 7 shows the lattice parameters as a function of incidence angle at V_{ds}=-20 V. The parameter b appears lower for the lowest incidence angle 0.20° and this may be an evidence for discontinuity of the crystalline structure at the surface. This effect of incidence angle is different for different lattice parameters, which implies that the effect is not an artefact. Any variation for $\geq$0.25° falls within the statistical error. Regardless the voltage, the nominal incidence angles 0.25-0.30° maximized the measured scattering intensities (and minimized the statistical error) and was used in the ageing studies below.

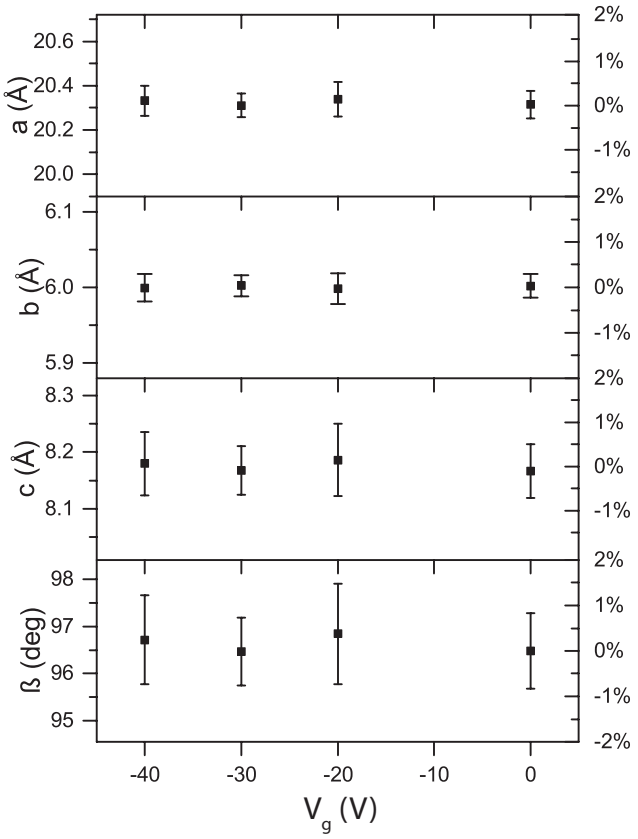

Figure 6: Lattice parameters of NaT2 as a function of V_g at 0.25° incidence angle. $V_{ds} = V_g$.

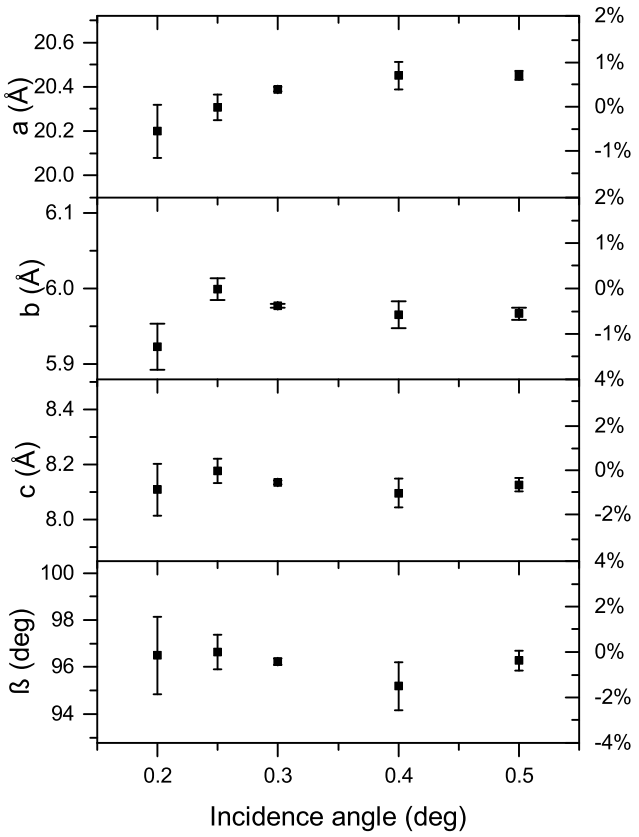

Figure 7: Lattice parameters of NaT2 as a function of incident angle with V_{ds}=-20 V and V_g=0 V

3.2. NaT2 structure and the OFET performance upon ageing.

Fig. 8 shows the lattice parameters of NaT2 in a running OFET with time. Fig. 9 shows the electrical characteristics of the same OFET measured simultaneously with the data shown in Fig. 7. The lattice parameters vary less than 1% when OFETs are cycled with V_g cycled between 0 V and -40 V and the cycling is continued over more than a 10 h period under inert gas conditions.

Simultaneous measurements of charge carrying capacities show that IV curves remain stable, with hole mobilities reaching stables level with an average of

$(3.25 \pm 0.04) \times 10^{-4}$ cm^2/Vs within a few cycles. For the remainder of the 10 h period mobility values varies less than 4% (including one standard deviation) from the average. These hole mobilities are more than an order of magnitude lower than the values reported by Geng and coworkers [21]. However, our films were deposited with the substrate at room temperature, while these authors used a substrate heated up to 80° C [21]. This may have a significant influence on thin-film morphology and thus also on the electrical transport properties. Furthermore, while Geng and co-workers employed a top contact configuration, we used a bottom contact configuration, which may result in a higher contact resistance that potentially can influence the extracted mobility.

Similarly, the threshold voltage shifts in the direction of the applied gate voltage during the first few cycles and then stabilize around an average value of -13.6 ± 0.2 V, varying less than 4% (including one standard deviation) from the average. This is in agreement with previous studies on similar materials [7] and is linked to the trapping of charged species during transistor operation. We note that the X-ray illumination during the GIXRD data collection can lead to charge detrapping that could affect the electrical characteristics [13]. However, since we report changes in electrical performance based on consecutive measurement using the exactly same measurement protocol, any potential changes are not due to X-ray induced photocurrent. However, in contrast to the results of Liscio and co-workers [13], we observe no correlation between the change in the thin film structure (Fig. 8) and electrical devices characteristics (Fig. 9). This suggests that the bias-stress instabilities do not have a structural origin in the unit cell level.

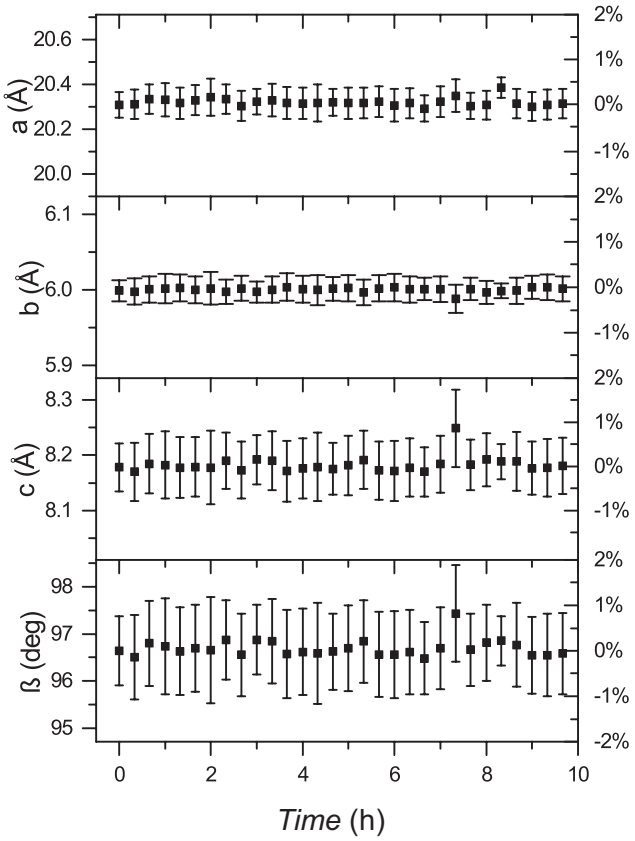

Figure 8: Lattice parameters of NaT2 in a cycled OFET as a function of time

4. Conclusions

NaT2 maintains its bulk monoclinic structure in operating OFETs with $a = 20.31 \pm 0.06$ Å, $b = 6.00 \pm 0.01$ Å, $c = 8.17 \pm 0.04$ Å and $\beta = (96.64 \pm 0.74)^\circ$ showing alignment out-of-plane but not in-plane. This together with the fact that the crystallite size along the **z** direction of ∼40 nm corresponds to the 50 nm film thickness indicate that NaT2 appears essentially as a mosaic of single crystals reaching through the whole active layer. NaT2 maintains its structure in OFETs where the lattice parameters vary less than 1% when incidence angle is varied from 0.25° to 0.5° and less than 1% when OFETs are cycled with V_g from 0 V to -40 V or when the cycling is continued over more than 10 h period under inert gas. At the same time hole mobility reaches stable levels within a few cycles with an average of $(3.25 \pm 0.04) \times 10^{-4}$ cm^2/Vs

and an average threshold voltage of -13.6 ± 0.2 V. Both the hole mobility and the threshold voltage varies less than 4% for the remainder of the 10 h period. These findings provide a structural insight into NaT2 OFETs. They confirm the assumption of NaT2 as stable OFET materials [21] and demonstrate the use of GIXRD when probing OFETs *in operando*.

Future studies should expand these experiments to Na2T nanofibers [23] and other naphtyl substituted oligothiophenes and surface effects as shown elsewhere for α,ω–dihexylsexithiophenes and other materials [16, 38]. They may also benefit from reflectivity experiments as demonstrated for polythiophenes elsewhere [39].

5. Acknowledgements

We thank Arne Lützen and Andreas Osadnik of the University of Bonn for providing NaT2; Michael J. Winokur of the University of Wisconsin-Madison and Thomas P. A. Hase of the University of Warwick for discussions; as well as the EPSRC funded XMaS mid-range facility, DANSCATT, the SDU2020 program, and the Danish Council for Independent Research for financial support.

References

[1] H. Sirringhaus, 25th anniversary article: Organic field-effect transistors: The path beyond amorphous silicon, Adv. Mater. 26 (2014) 1319–1335.

[2] S. Holliday, J. E. Donaghey, I. McCulloch, Advances in charge carrier mobilities of semiconducting polymers used in organic transistors, Chem. Mater. 26 (2014) 647–663.

[3] T. H. Lee, K. Kim, G. Kim, H. J. Park, D. Scullion, L. Shaw, M.-G. Kim, X. Gu, W.-G. Bae, E. J. G. Santos, Z. Lee, H. S. Shin, Y. Nishi, Z. Bao, Chemical vapor-deposited hexagonal boron nitride as a scalable template for high-performance organic field-effect transistors, Chem. Mater. 29 (2017) 2341–2347.

[4] A. N. Sokolov, S. Atahan-Evrenk, R. Mondal, H. B. Akkerman, R. S. Sánchez-Carrera, S. Granados-Focil, J. Schrier, S. C. Mannsfeld, A. P. Zoombelt, Z. Bao, A. Aspuru-Guzik, From computational discovery to

experimental characterization of a high hole mobility organic crystal, Nature Comm. 2 (2011) 437.

[5] Y. Yuan, G. Giri, A. L. Ayzner, A. P. Zoombelt, S. C. B. Mannsfeld, J. Chen, D. Nordlund, M. F. Toney, J. Huang, Z. Bao, Ultra-high mobility transparent organic thin film transistors grown by an off-centre spin-coating method, Nature Comm. 5 (2014) 3005.

[6] D. Li, E.-J. Borkent, R. Nortrup, H. Moon, H. Katz, Z. Bao, Humidity effect on electrical performance of organic thin-film transistors, Appl. Phys. Lett. 86 (2005) 042105.

[7] W. H. Lee, H. H. Choi, D. H. Kim, K. Cho, 25th anniversary article: Microstructure dependent bias stability of organic transistors, Adv. Mater. 26 (2014) 1660–1680.

[8] M. Tello, M. Chiesa, C. M. Duffy, H. Sirringhaus, Charge trapping in intergrain regions of pentacene thin film transistors, Adv. Funct. Mater. 18 (2008) 3907–3913.

[9] R. Häusermann, B. Batlogg, Gate bias stress in pentacene field-effect-transistors: Charge trapping in the dielectric or semiconductor, Appl. Phys. Lett. 99 (2011) 083303.

[10] S. G. Mathijssen, M.-J. Spijkman, A.-M. Andringa, P. A. van Hal, I. McCulloch, M. Kemerink, R. A. J. Janssen, D. de Leeuw, Revealing buried interfaces to understand the origins of threshold voltage shifts in organic field-effect transistors, Adv. Mater. 22 (2010) 5105–5109.

[11] G. Gu, M. G. Kane, Moisture induced electron traps and hysteresis in pentacene based organic thin-film transistors, Appl. Phys. Lett. 92 (2008) 053305.

[12] P. A. Bobbert, A. Sharma, S. G. J. Mathijssen, M. Kemerink, Operational stability of organic field-effect transistors, Adv. Mater. 24 (2012) 1146–1158.

[13] F. Liscio, L. Ferlauto, M. Matta, R. Pfattner, M. Murgia, C. Rovira, M. Mas-Torrent, F. Zerbetto, S. Milita, F. Biscarini, Changes of the molecular structure in organic thin film transistors during operation, J. Phys. Chem. C 119 (2015) 15912–15918.

[14] B. Kumar, B. K. Kaushik, Y. S. Negi, Organic thin film transistors: Structures, models, materials, fabrication, and applications: A review, Polym. Rev. 54 (2014) 33–111.

[15] Y. Liu, C.-a. Di, C. Du, Y. Liu, K. Lu, W. Qiu, G. Yu, Synthesis, structures, and properties of fused thiophenes for organic field-effect transistors, Chem. Eur. J. 16 (2010) 2231–2239.

[16] E. M. Mannebach, J. W. Spalenka, P. S. Johnson, Z. Cai, F. J. Himpsel, P. G. Evans, High hole mobility and thickness-dependent crystal structure in α,ω–dihexylsexithiophene single-monolayer field-effect transistors, Adv. Funct. Mater. 23 (2012) 554–564.

[17] T. J. Shin, H. Yang, M.-m. Ling, J. Locklin, L. Yang, B. Lee, M. E. Roberts, A. B. Mallik, Z. Bao, Tunable thin-film crystalline structures and field-effect mobility of oligofluorene-thiophene derivatives, Chem. Mater. 19 (2007) 5882–5889.

[18] T. K. An, J. H. Jang, S.-O. Kim, J. Jang, J. Hwang, H. Cha, Y. R. Noh, S. B. Yoon, Y. J. Yoon, L. H. Kim, D. S. Chung, S.-K. Kwon, Y.-H. Kim, S.-G. Lee, C. E. Park, Synthesis and transistor properties of asymmetric oligothiophenes: Relationship between molecular structure and device performance, Chem. Eur. J. 19 (2013) 14052–14060.

[19] S. R. Walter, J. Youn, J. D. Emery, S. Kewalramani, J. W. Hennek, M. J. Bedzyk, A. Facchetti, T. J. Marks, F. M. Geiger, In-situ probe of gate dielectric-semiconductor interfacial order in organic transistors: Origin and control of large performance sensitivities, J. Am. Chem. Soc. 134 (2012) 11726–11733.

[20] T. Kubo, R. Häusermann, J. Tsurumi, J. Soeda, Y. Okada, Y. Yamashita, N. Akamatsu, A. Shishido, C. Mitsui, T. Okamoto, S. Yanagisawa, H. Matsui, J. Takeya, Suppressing molecular vibrations in organic semiconductors by inducing strain, Nature Comm. 7 (2016) 11156.

[21] H. Tian, J. Shi, B. He, N. Hu, S. Dong, D. Yan, J. Zhang, Y. Geng, F. Wang, Naphtyl and thionaphtyl end-capped oligothiophenes as organic semiconductors: Effect of chain length and end-capping groups, Adv. Funct. Mater. 17 (2007) 1940–1951.

[22] X. Liu, L. Tavares, A. Osadnik, J. L. Lausen, J. Kongsted, A. Lützen, H.-G. Rubahn, J. Kjelstrup-Hansen, Low-voltage organic phototransistors based on naphthyl end-capped oligothiophene nanofibers, Org. Electron. 15 (2014) 1273–1281.

[23] F. Balzer, M. Schiek, A. Osadnik, I. Wallmann, J. Parisi, H.-G. Rubahn, A. Lützen, Subtrate steered crystallization of napthyl end-capped oligothiophenes into nanofibers: The influence of methoxy-functionalization, Phys. Chem. Chem. Phys. 16 (2014) 5747–5754.

[24] H. Sirringhaus, P. J. Brown, R. H. Friend, M. M. Nielsen, K. Bechgaard, B. M. W. Langeveld-Voss, A. J. H. Spiering, R. A. J. Janssen, E. W. Meijer, P. Herwig, D. M. de Leeuw, Two-dimensional charge transport in self-organized, high-mobility conjugated polymers, Nature 401 (1999) 685–688.

[25] C. D. Liman, S. Choi, D. W. Breiby, J. E. Cochran, M. F. Toney, E. J. Kramer, M. L. Chabinyc, Two-dimensional giwaxs reveals a transient crystal phase in solution-processed thermally converted tetrabenzoporphyrin, J. Phys. Chem. B 117 (2013) 14557–14567.

[26] M. Knaapila, B. P. Lyons, T. P. A. Hase, C. Pearson, M. C. Petty, L. Bouchenoire, P. Thompson, R. Serimaa, M. Torkkeli, A. P. Monkman, Influence of the molecular weight on the surface morphology of aligned, branched side chain polyfluorene, Adv. Funct. Mater. 15 (2005) 1517–1522.

[27] G. Giri, R. Li, D.-M. Smilgies, E. Q. Li, Y. Diao, K. M. Lenn, M. Chiu, D. W. Lin, R. Allen, J. Reinspach, S. C. B. Mannsfeld, S. T. Thoroddsen, P. Clancy, Z. Bao, A. Amassian, One-dimensional self-confinement promotes polymorph selection in large-area organic semiconductor thin films, Nature Comm. 5 (2014) 3573.

[28] H. U. Khan, R. Li, Y. Ren, L. Chen, M. M. Payne, U. S. Bhansali, D.-M. Smilgies, J. E. Anthony, A. Amassian, Solvent vapor annealing in the molecular regime drastically improves carrier transport in small-molecule thin-film transistors, ACS Appl. Mater. & Interfaces 5 (2013) 2325–2330.

[29] A. P. L. Böttiger, M. Jørgensen, A. Menzel, F. C. Krebs, J. W. Andreasen, High-throughput roll-to-roll x-ray characterization of polymer solar cell active layers, J. Mater. Chem. 22 (2012) 22501–22509.

[30] M. Sanayal, B. Schmidt-Hansberg, M. F. G. Klein, C. Munuera, A. Vorobiev, A. Colsmann, P. Scharfer, U. Lemmer, W. Schabel, H. Dosch, E. Barrena, In situ x-ray study of drying-temperature influence on the structural evolution of bulk-heterojunction polymer-fullerene solar cells processed by doctor-blading, Adv. Energy Mater. 1 (2011) 363–367.

[31] S. V. Roth, A deep look into the spray coating processin real-time - the crucial role of x-rays, J. Phys.: Condens. Matter 28 (2016) 403003.

[32] X. Liu, I. Wallmann, H. Boudinov, J. Kjelstrup-Hansen, M. Schiek, A. Lützen, H.-G. Rubahn, Ac-biased organic light-emitting field-effect transistors from naphthyl end-capped oligothiophenes, Org. Electron. 15 (2010) 1273–1281.

[33] S. Lilliu, J. Griffin, A. T. Barrows, M. Alsari, B. Curzadd, T. G. Dane, O. Bikondoa, J. E. Macdonald, D. G. Lidzey, Grain rotation and lattice deformation during perovskite spray coating and annealing probed in situ by gi-waxs, CrystEngComm. 18 (2016) 5448–5455.

[34] C. M. Schlepütz, S. O. Mariager, S. A. Pauli, R. Feidenhans'l, P. R. Willmott, Angle calculations for a (2+3)-type diffractometer: focus on area detectors, J. Appl. Cryst. 44 (2011) 73–83.

[35] J. L. Baker, L. H. Jimison, S. Mannsfeld, S. Volkman, S. Yin, V. Subramanian, A. Salleo, A. P. Alivisatos, M. F. Toney, Quantification of thin film crystallographic orientation using x-ray diffraction with an area detector, Langmuir 26 (2010) 9146–9151.

[36] S. E. Fritz, S. M. Martin, C. D. Frisbie, M. D. Ward, M. F. Toney, Structural characterization of a pentacene monolayer on an amorphous sio2 substrate with grazing incidence x-ray diffraction, J. Am. Chem. Soc. 126 (2004) 4084–4085.

[37] H. Yang, T. J. Shin, M.-M. Ling, K. Cho, C. Y. Ryu, Z. Bao, Conducting afm and 2d gixd studies on pentacene thin films, J. Am. Chem. Soc. 127 (2005) 11542–11543.

[38] A. O. F. Jones, B. Chattopadhyay, Y. H. Geerts, R. Resel, Substrate-induced and thin-film phases: Polymorphism of organic materials on surfaces, Adv. Funct. Mater. 26 (2016) 2233–2255.

[39] N. Jian, L. Sendogdular, M. Sen, M. K. Endoh, T. Koga, M. Fakuto, B. Akgun, S. K. Satija, C.-Y. Nam, Novel effects of compressed co2 molecules on structural ordering and charge transport in conjugated poly(3-hexylthiophene) thin films, Langmuir 32 (2016) 10851–10560.

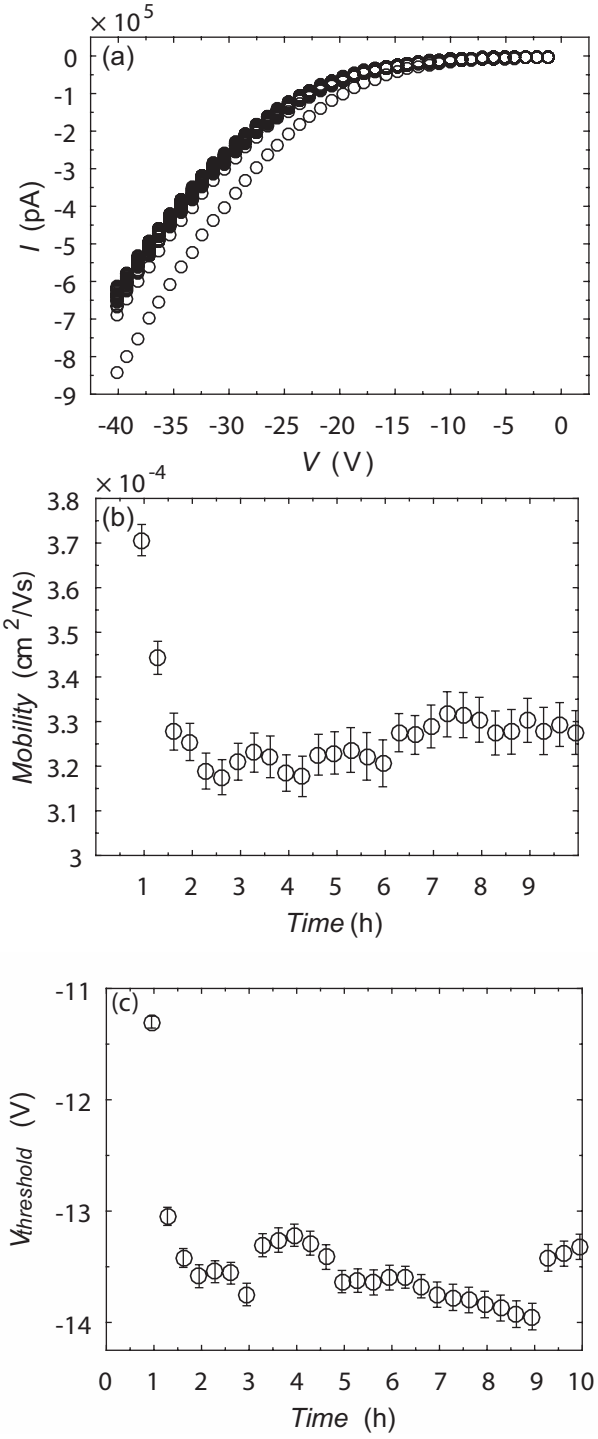

Figure 9: (a) I-V curves and (b) hole mobilities and (c) threshold voltage of NaT2 in a cycled OFET as a function of time measured simultaneously with the data shown in Fig. 8